Analysis of the interactions between close HVDC links inserted in an AC grid

Iulian Munteanu, Bogdan Marinescu, Florent Xavier

Analysis of the interactions between close HVDC links inserted in an AC grid

Iulian Munteanu
École Centrale Nantes – IRCCYN
Nantes, France
Email: iulian.munteanu@ec-nantes.fr

Bogdan Marinescu
École Centrale Nantes – IRCCYN
Nantes, France
Email: bogdan.marinescu@ec-nantes.fr

Florent Xavier
Réseau de Transport d'Électricité
Versailles, France
Email: florent.xavier@rte-france.com

***Abstract*—This paper is focused on interaction between two closed-connected high-voltage DC (HVDC) lines. This interaction is studied by employing electromagnetic transients (EMT)–based nonlinear modeling in MATLAB®/Simulink® software environment. In order to describe the mechanism behind the HVDCs interaction, both nonlinear time-domain simulations and modal analysis of the coupled HVDC links, using linearized version of the system, have been performed. System stability has been assessed and the path of interactions has been identified by computing the participations of various states in the oscillatory modes.**

I. Introduction

Being flexible electrical power transmission structures able to convey large amount of power, high-voltage DC (HVDC) links may be used to connect two areas of the AC power grid to reinforce transmission capacity [1]. As two lines may be connected in areas having weak AC grid, their operation are likely to interfere due to geographic proximity, with potentially negative effects on their stability.

Parallel VSCs operation in AC grid context is studied in [2], and overall system stability is assessed by employing input-admittance modeling the converters. In [3] control solutions are proposed to diminish interaction between two close HVDCs using simplified phasor models. The present work develops the analysis of these interactions by using electromagnetic transients (EMT)-based modeling which captures the high-frequency VSC average behavior.

The approached system structure consists of two two-level HVDCs interconnected by means of a common AC power line, further denoted as ConAC – see Fig. 1. This is derived from the benchmark in [4], all AC lines and generators being simplified to impedances and infinite nodes. The simplification allows to better identify dynamic properties belonging exclusively to HVDCs coupling. Also, system behavior is assessed by means of modal analysis for continuous-time linear systems – [5], which offers a tool of determining the degree of participation of system states in a certain (oscillatory) mode. Originally used for stability issues in classical power system analysis, this approach may be applied to other types of complex systems, in which decoupling methods cannot be employed. A similar approach using multimodular converter (MMC)-based HVDC has been briefly presented in [6]. The present work extends system evaluation by thoroughly assessing states influence in shaping HVDC's interaction for various operating scenarios.

The paper is organized as follows. Section II goes on with HVDC line modeling aspects, while Section III presents nonlinear time-domain simulation and modal analysis results. Section IV concludes the paper.

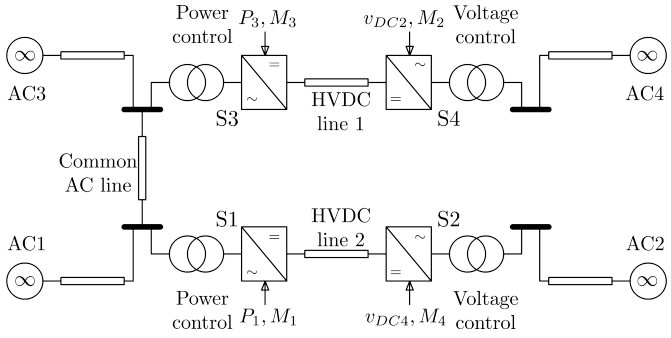

Fig. 1. Interconnection of two HVDC lines by means of an AC line.

II. Modeling approach

A. HVDC structure and assumptions

VSC-HVDC transmission power structure (Fig. 2) corresponds to a monopolar structure with metallic return. It has two conversion stations that employ bidirectional 3-phased AC-DC power converters, interlinked by means of DC cables and connected to AC grids trough step-up transformers. VSC switched operation requires filtering elements on each station: capacitors on DC side and line reactors on AC side.

The following assumptions are considered. AC-DC converters are lossless and are switching instantaneously at a sufficiently high frequency; so the low-pass filter (habitually inserted between line reactor and transformer) is neglected. DC filter is reduced to capacitors, AC transformer has negligible magnetizing impedance and magnetic saturation phenomena are not considered. AC environment is modeled by AC infinite buses and variable series reactances; it is symmetrical and balanced. The common AC line is modeled as an RL circuit element. VSCs of HVDC link are operated in pulse-width modulation (PWM) in order to interchange averaged sinusoidal variables with AC grid. As this work is focused on the HVDCs low-frequency behavior, VSCs are modeled here by their averaged model, obtained by replacing converter switching functions with their sliding averages [7].

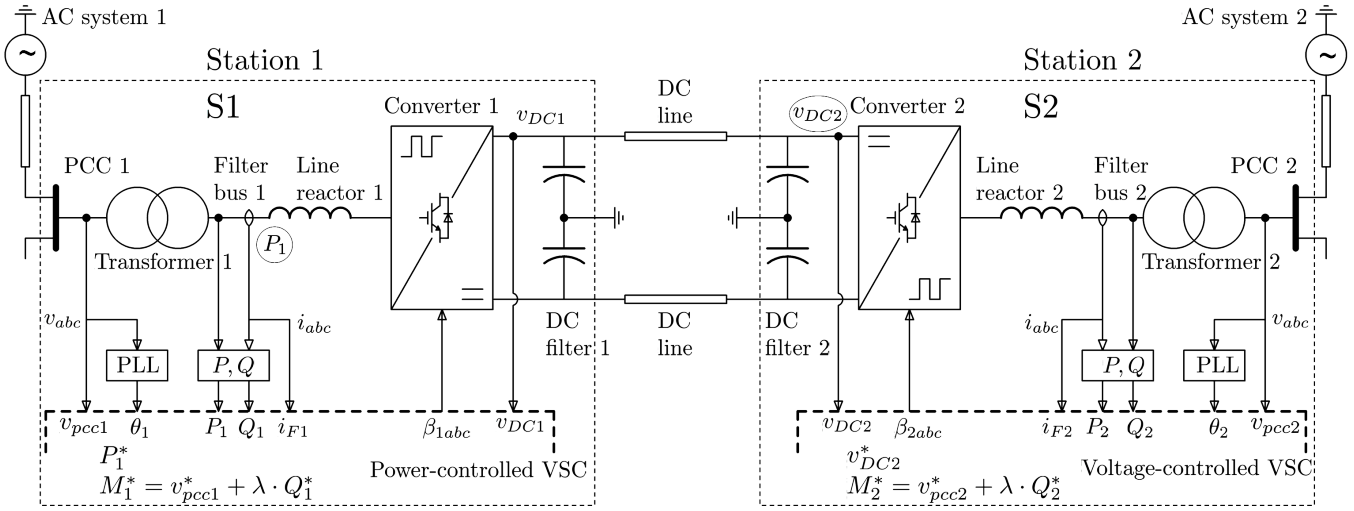

Fig. 2. HVDC transmission line overall control.

B. dq frame modeling

The power subsystem (plant) model results from describing the electrical interactions between VSC and infinite node through passive circuit elements. First, one obtains an equivalent circuit by pushing the transformer primary inductance into the secondary (see Fig. 2 and transformer modeling in [7]); the whole AC system (including infinite nodes) becomes rated at VSC voltage value. Model is then described in rotating *dq* frame linked to the infinite node; d channel conveys active power and q channel reactive power.

The plant model in this *dq* frame is given by (1) – see [8],[9], where i_{rd} and i_{rq} are equivalent AC inductor current components, i_{ld} and i_{lq} are AC line components, v_{rd} and v_{rq} are the point of common coupling (PCC) voltage components, E is the infinite node voltage amplitude, ω is AC system frequency and v_{DC} is DC line voltage at the concerned VSC (capacitor filter voltage). L_r and r_r are reactor inductance and resistance, respectively, L_l and r_l are AC line inductance and resistance, respectively and C is value of DC-side capacitors. β_{rd} and β_{rq} are plant control inputs. Voltage v_{rd} is obtained by balancing currents i_{rd} and i_{ld} on a small resistive charge, R_D: $v_{rd} = (i_{ld} - i_{rd}) \cdot R_D$.

The same remark applies for channel q.

$$\begin{cases} L_r \cdot \dot{i_{rd}} = \omega L_r \cdot i_{rq} - 0.5 v_{DC} \cdot \beta_{rd} + v_{rd} - r_r \cdot i_{rd} \\ L_r \cdot \dot{i_{rq}} = -\omega L_r \cdot i_{rd} - 0.5 v_{DC} \cdot \beta_{rq} + v_{rq} - r_r \cdot i_{rq} \\ L_l \cdot \dot{i_{ld}} = \omega L_l \cdot i_{lq} - v_d + E - r_l \cdot i_{ld} \\ L_l \cdot \dot{i_{lq}} = -\omega L_l \cdot i_{ld} - v_q - r_l \cdot i_{rq} \\ C \cdot \dot{v_{DC}} = 1.5 \left(i_{rd} \cdot \beta_{rd} + i_{rq} \cdot \beta_{rq} \right) - i_{dc} \\ L_{dc} \cdot \dot{i_{dc}} = v_{DC} - v_{DCr} - r_{dc} \cdot i_{dc} \end{cases} \tag{1}$$

Classical VSC control in the *dq* frame linked to the PCC by means of a phase locked loop (PLL) [9], is used here, in which proportional-integral-law-based inner current control loops are cross-decoupled [8], [9]. On d channel, either active power at PCC or DC-link voltage are controlled within an outer loop. On q channel a mix between the PCC voltage and reactive power, Q is controlled in a second outer loop – see [10]. This is here represented by variable $M = v_{PCC} + \lambda \cdot Q$, λ being the reactive power coefficient (kV/kVar).

$$\begin{cases} \beta_d = -K_{pc} \left(1 + \dfrac{1}{T_{ic} s} \right) \left(\dfrac{i_d^*}{T_{ic} s + 1} - i_d \right) + \dfrac{2 \omega L_r}{v_{DC}} \cdot i_q \\ \beta_q = -K_{pc} \left(1 + \dfrac{1}{T_{ic} s} \right) \left(\dfrac{i_q^*}{T_{ic} s + 1} - i_q \right) - \dfrac{2 \omega L_r}{v_{DC}} \cdot i_d \\ i_d^* = \dfrac{1}{T_{iP} s} \cdot (P^* - P) \,;\; i_q^* = \dfrac{1}{T_{iM} s} \cdot (M^* - M) \\ P = 1.5 \left(v_d \cdot i_d + v_q \cdot i_q \right) \,;\; Q = 1.5 \left(v_d \cdot i_q - v_q \cdot i_d \right) \end{cases} \tag{2}$$

The overall control law expressed in *dq* frame linked to PCC is given by (2) – see [6], [8] – where i_d and i_q are measured reactor current components, v_d and v_q are voltages measured at PCC, P and Q are PCC active and reactive power components and s is the Laplace operator. Variables $\langle \cdot^* \rangle$ denote the associated setpoints. K_{pc} and T_{ic} are the proportional gain and integrator constant of PI current controllers, T_{iP} is the active power controller integrator constant and T_{iM} is the reactive power controller integrator constant. The third equation of (2) is valid only for the power-controlled station/VSC. Stations with (DC) voltage control employ (3) instead.

$$i_d^* = K_{pv} \left(1 + \frac{1}{T_{iv} s} \right) \cdot (v_{DC}^* - v_{DC}) \tag{3}$$

In order to render variables from the control and power structures compatible, one must make a rotation transform from the PCC-linked frame to the infinite-node-linked frame. This is done by using the Kron's transform [11], which uses the phase shift between the two frames, denoted by δ:

$$\begin{cases} i_d = i_{rd} \cdot \cos\delta - i_{rq} \cdot \sin\delta \\ i_q = i_{rd} \cdot \sin\delta + i_{rq} \cdot \cos\delta \\ \beta_{rd} = \beta_d \cdot \cos(-\delta) - \beta_q \cdot \sin(-\delta) \\ \beta_{rq} = \beta_d \cdot \sin(-\delta) + \beta_q \cdot \cos(-\delta) \end{cases} \quad (4)$$

PCC phase angle is extracted from its voltages by using a 3-phase PLL. PLL angle serves for all computations in the station control system, but its value is delayed with respect to the PCC angle. The overall dynamic behavior of the controlled VSC, is thus impacted – see [12]. In this work, a new PLL structure has been used – see Fig. 3, which has exactly the same dynamics as 1th order classical PLL. It outputs not only PCC voltage components v_d and v_q, but also the phase shift δ. PLL dynamics intervene twice: in i_d and i_q measurement and in β_{rd} and β_{rq} actuation by means of angle δ.

Further, stations S1 and S3 (see Fig. 1) are modeled by using (1) and (2), *i.e.*, they are power-controlled, and stations S2 and S4 use (1) and (2), where the third equation is replaced by (3), *i.e.*, they are voltage-controlled. ConAC line is modeled as a RL line, by using the equations similar to the two first equations from (1).

The control system of a single HVDC line is tuned to obtain pertinent performances for i_d and i_q: damping at around 0.65 - 0.85 and time constant 5 ms for the inner loops, for typical scenarios and operating points. Time constant for outer loops is around 17 ms for v_{DC} control loop and 20 - 30 ms for active power P and variable M. All these outer loops have variable damping depending on grid equivalent short-circuit ratio (SCR) and on the operating point.

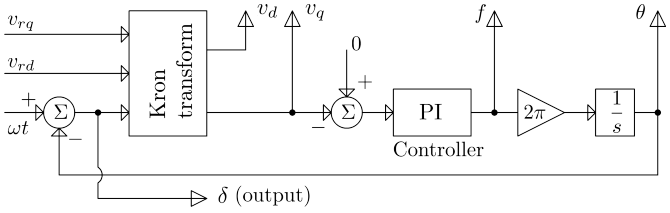

Fig. 3. PLL structure using Kron's transform as phase detector; steady-state value of δ nullifies voltage v_q.

C. System linearization and modal analysis

All system states (integrators) are labeled with suitable keywords (*e.g.*, "int PI id2" means the state associated with the i_{d2} current controller integrator). Linearization is done by using the *Linear analysis* tool available in MATLAB®/Simulink® software around a suitable steady-state operating point. In all results in this section the input is chosen as M_1^* (the setpoint) and the output as M_1, although any of variables P_k and M_k with $k = 1..4$, may be set as output.

Modal analysis for continuous-time linear time-invariant system starts with the state matrix, denoted by A, previously obtained by linearization. Then, normalized right eigenvectors v_i and left eigenvectors w_i, which verify that

$$\begin{cases} A \cdot v_i = v_i \cdot \lambda_i \\ w_i \cdot A = \lambda_i \cdot w_i, \end{cases} \quad (5)$$

with $w_i \cdot v_j = 0$ for $i \neq j$ and $w_i \cdot v_j = 1$ for $i = j$ – see [5] – are determined, where λ_i are the state matrix A eigenvalues.

The participation factor of variable x_j in mode i is computed as the product between elements j of vectors w_i and v_i – see [5] for quick reference :

$$p_{ji} = (w_i)_j \cdot (v_i)_j . \quad (6)$$

One determines participation factors for all state variables and for all system modes, resulting values form the so-called participation factor matrix (square matrix of system dimension) [5]. Absolute values of participation factors are further used, in order to compare variables that intervene in a certain mode. The modes of interest are chosen by using damping criterion *i.e.*, the ones having the damping under a certain threshold, in order to emphasize system oscillations/couplings.

III. Analysis results

A. Nonlinear time-domain simulations

In all subsequent scenarios, only parameters/setpoints of stations S1 and S3 will change; stations S2 and S4 setpoints are $v_{DC2} = v_{DC4} = 640$ kV and $M_2 = M_4 = 332$ kV. Their associated SCR is always constant, at ≈ 5. Also, the values considered for ConAC line length correspond to the initially-stated "close" HVDC lines context.

The first scenario consists in injecting active power values $P_1 = -500$ MW and $P_3 = -250$ MW and maintaining $M_1 = M_3 = 332$ kV (*i.e.*, at their rated values), for various ConAC line lengths – see Figs. 4 a) and b). Both S1 and S3 have the same SCR=5 value. A large step of M_1 setpoint (≈ 500 MVar of reactive power), has been imposed.

Fig. 4 a) presents M_1 evolutions (local control loop voltage tracks setpoint variation), and Fig. 4 b) M_3 evolutions – corresponding control loop rejects the perturbation. System's dynamic behavior has two main components: a damped behavior whose frequency becomes smaller as ConAC line length decreases, and a second undamped behavior, whose frequency is around 20 Hz and which is the target of the subsequent modal analysis.

In Fig. 4 c) a detail of M_1 (black) and M_3 (red) evolutions at a M_1 setpoint step (ConAC is of 100 km) is shown. The same transient dynamics can be noted on both outputs – oscillations have the same frequency, the same damping and the same phase, suggesting that the two input-output transfer channels are coupled, as their oscillations are due to the same mode.

Fig. 4 d) shows M_3 evolution at a step in M_1 setpoint, within a different scenario, with various SCR values at both stations S1 and S3 and constant ConAC line length at 150 km. S1 and S3 setpoints are the same as in the previous scenario. The system is less damped as SCRs values at both S1 and S3 are smaller (the grid is weaker). If one continues to reduce SCR values, the system becomes unstable.

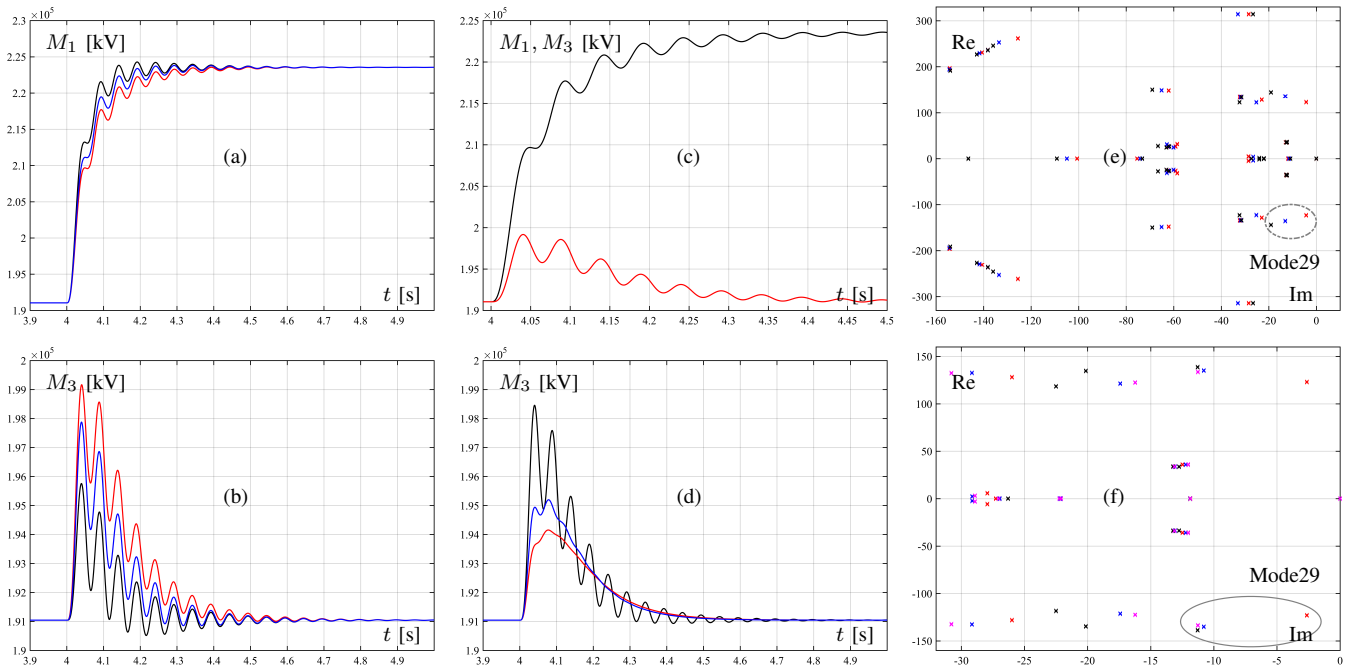

Fig. 4. a) and b): system response at M_1 stepoint step variation, for various ConAC line lengths black – 500 km, blue – 200 km, red – 100 km, (a) M_1 evolution, b) M_3 evolution); c): detail of M_1 (black) and M_3 (red) evolutions at a M_1 setpoint step (ConAC is of 100 km); d): M_3 evolution at M_1 stepoint step variation, for various SCR values (black – 7.5, blue – 5, red – 3.5); e): system pole-zero maps for various SCR values: black – 5, blue – 4, red – 3; f): system pole-zero maps for various P_1 and P_3 setpoints; red: $P_1 = -500$ MW, $P_3 = -600$ MW, blue: $P_1 = -500$ MW, $P_3 = +600$ MW, magenta: $P_1 = +500$ MW, $P_3 = -600$ MW, black $P_1 = +500$ MW, $P_3 = +600$ MW.

TABLE I
Mode 29 PARAMETERS VARIATIONS: LEFT SIDE – WITH SCR VALUES, RIGHT SIDE – WITH P_1 AND P_3 VALUES.

SCR	Freq. [Hz]	Damp.	P_1, P_3 [MW]	Freq. [Hz]	Damp.
3	19.6	0.034	-500, -600	19.57	0.021
4	21.6	0.096	-500, +600	21.5	0.08
5	22.94	0.131	+500, -600	21.27	0.084
-	-	-	+500, +600	22.08	0.081

TABLE II
STATES INFLUENCES IN *Mode 29* FOR TWO VALUES OF SCR.

SCR →	4	SCR →	3
State name	Participation	State name	Participation
int PI iq1	0.09	int PLL1	0.15
int PLL1	0.09	int PI iq1	0.14
int PI iq3	0.09	int PLL3	0.13
int PLL3	0.08	int PI iq3	0.13
int PI id1	0.06	int PI id3	0.09
Reactor 1/int2	0.07	int PI id1	0.1
Reactor 3/int2	0.05	Reactor 1/int2	0.09
int PI id4	0.05	Reactor 3/int2	0.07
int PLL4	0.05	int PI PLL1	0.06
int PI iq4	0.05	AC line 1/int2	0.05

B. Modal analysis

For each scenario the nonlinear system is linearized around the associated steady-state operating point, by using MATLAB®/Simulink®; thus, a 62-state linear model is obtained. Modal analysis algorithm – based upon equations (5) and (6) – is applied and the previously-observed oscillatory mode (see Fig. 4) is identified. It will be further referred to as *Mode 29*.

The first scenario involves modal analysis for three different SCR values at stations S1 and S3. Steady-state active power values are $P_1 = -500$ MW and $P_3 = -250$ MW, M variables $M_1 = M_3 = 332$ kV and ConAC line length is 150 km.

Table I (left side) shows *Mode 29* main parameters for the three SCR values. Frequency has not an important variation, but the damping is severely decreasing with SCR, thus affecting the system stability. Fig. 4 e), which contains the system pole's evolution as SCR decreases (only low-frequency complex-conjugated poles have been plotted), shows the same trend. Table II contains ranking of most participative system states in *Mode 29* for two values of SCR. Variables belonging to S1 – from the HVDC link 1 – and S3 – from the HVDC link 2 – have the most important contribution to the concerned mode. This proves that the two HVDCs are interacting.

The second scenario concerns modal analysis for various active power values (positive/power draw or negative/power injection) required for stations S1 and S3. The set-up presumes a ConAC line of 150 km, both S1 and S3 maintain variables M_1 and M_3 at their rated values (*i.e.*, 332 kV); SCR is the same for S1 and S2, *i.e.*, 3.5. Stations S2 and S4 follow operation of stations S1 and S3 respectively, by regulating DC voltage at the rated value (640 kV).

Table I (right side) shows *Mode 29* parameters variation

TABLE III
STATES WITH LARGEST PARTICIPATION IN *Mode 29* FOR VARIOUS P_1 AND P_3 VALUES.

P_1=-500, P_3=-600	[MW]	P_1=+500, P_3=+600	[MW]	P_1=+500, P_3=-600	[MW]	P_1=-500, P_3= +600	[MW]
State name	Part.	State name	Part.	State name	Part.	State name	Part.
int PLL1	0.13	int PI iq4	0.07	int PI id2	0.17	int PI id4	0.14
int PLL3	0.13	int PI id4	0.07	int PLL2	0.15	int PLL4	0.12
int PI iq3	0.13	int PLL4	0.07	int PI iq2	0.14	int PI iq4	0.12
int PI iq1	0.12	int PI id2	0.06	int PLL3	0.1	Reactor 4/int 2	0.09
int PI id3	0.1	int PLL2	0.06	int PI iq3	0.1	int PLL1	0.07
int PI id1	0.09	int PI iq2	0.05	Reactor 2/int 2	0.1	int PI iq1	0.07
Reactor 3/int 2	0.08	Reactor 4/int 2	0.05	Reactor 2/int 1	0.09	Reactor 4/int1	0.07
Reactor 1/int 2	0.08	Reactor 2/int 2	0.04	AC line 2/int1	0.07	Prefilter id4	0.06
AC line 3 /int 2	0.05	int PLL1	0.04	Prefilter id2	0.07	AC line 4 /int1	0.06
int PI PLL3	0.05	int PI iq1	0.04	Reactor 3/int2	0.07	Reactor 1/int 2	0.05

with P_1 and P_3 values. Damping of *Mode 29* is lowest when both S1 and S3 inject power in AC grid. This is also visible on Fig. 4 f), showing variation of pole associated with *Mode 29* with respect to power levels.

Ranking of first ten states participating in *Mode 29* are shown in Table III. The inner loop (current) controllers states, including PLLs (either the PLL integrator or its PI controller), have the most important participation in this mode. Note also, that these states belong to stations that inject active power. For example, ranking in column 3 of Table III, corresponds to case where S1 draws power and S3 injects power from/in their AC grids. Therefore, S2 injects power and S4 draws power in/from their AC grids in order to maintain DC voltage at the prescribed value. States belonging to stations S2 and S3 are the most participative. This remark holds for all cases (see Table III). Also, notice that the coupling mode is systematically better damped in scenarios where power-controlled stations (S1 and S3) draw power – see the right side of Table I.

Note that in all cases the states belonging to the ConAC line do not significantly intervene in *Mode 29*. Also, states belonging to VSC reactors, AC lines and low-level loop prefilters – see equations (2) – may also be significantly involved in the participation mix.

IV. CONCLUSION

This paper has dealt with analysis of two close-connected HVDC lines by using high-fidelity models in *dq* frame.

A potentially inconvenient interaction, due to HVDCs coupling, has been highlighted by time-domain simulation. Also, modal analysis in various scenarios has revealed that low-level controllers states and PLL states significantly participate in the coupling oscillatory mode. The damping of coupling mode may be under 5% if both AC-linked stations inject active power into the grid. This damping becomes smaller as AC grid SCRs decrease.

Further work will focus to study interaction between HVDC links operating into richer AC environment which includes synchronous generators. Also, based upon this analysis, corrective control actions will be proposed.

APPENDIX. SYSTEM PARAMETERS

- AC system: frequency 50 Hz, rated RMS voltage 400 kV,
- AC line: resistance 0.03 Ω/km, inductance 0.79 mH/km,
- Transformer: secondary RMS voltage 230 kV, ratio 1.74, $R_{pr} = 0.4\ \Omega$, $L_{pr} = 38$ mH, $R_{sec} = 0.132\ \Omega$, $L_{sec} = 12.6$ mH,
- Line reactor: impedance 25.3 mH, resistance 0.08 Ω,
- DC line: voltage 640 kV, capacitor 220 μF, resistance 13.9 mΩ/km, impedance 0.159 mH/km, length 200 km,
- VSCs: active power 1000 MW, reactive power $Q \in \{-500; +400\}$ MVAr, maximum active current ± 4 kA, maximum reactive current ± 1.6 kA,
- Control parameters: λ=13e-6 V/VAr, $T_{ic} = 6.6$ ms, K_{pc}=0.6e-4 A^{-1}, $K_{tc} = 5 \cdot K_{tp} = 500$, $K_{pv} = 0.034$ A/V, $T_{iv} = 25$ ms, $T_{im} = 0.2845$ s, $T_{ip} = 7.04$ ms.

REFERENCES

[1] N. Flourentzou, V. G. Agelidis, and G. D. Demetriades, "VSC-Based HVDC Power Transmission Systems: An Overview," IEEE Trans Power Electron vol. 24, no. 3, pp. 592-602, 2009.

[2] A. Bayo-Salas, J. Beerten, J. Rimez, and D. Van Hertem, "Impedance-based stability assessment of parallel VSC HVDC grid connections," in the 11th IET International Conference on AC and DC Power Transmission, 10-12 February, Birmingham, UK, pp. 1-9, 2015.

[3] L. Arioua and B. Marinescu, "Multivariable control with grid objectives of an HVDC link embedded in a large-scale AC grid," Electrical Power and Energy Systems, vol. 72, 99-108, 2015.

[4] S. Henry, O. Despouys, R. Adapa and *al.*, "Influence of Embedded HVDC Transmission on System Security and AC Network Performance," Cigre JWG C4/B4/C1.604, 2013.

[5] G. Rogers, "Power system oscillations," Springer Science+Business Media, New York, USA, 2000.

[6] Saad HA, "Modeling and simulation of a VSC-MMC HVDC link" (in French: Modélisation et simulation d'une liaison HVDC de type VSC-MMC), PhD. Thesis, University of Montréal, Canada, 2015.

[7] R. W. Erikson and D. Maksimović "Fundamentals of power electronics, 2nd edn.," Kluwer, New York, USA, 2001.

[8] W. Wang, A. Beddard, M. Barnes, and O. Marjanovic, "Analysis of Active Power Control for VSC-HVDC," IEEE Trans. on Power Delivery, vol. 29, no. 4, pp:1978-1988, 2014.

[9] S. Bacha, I. Munteanu, A.I. Bratcu, "Power Electronic Converters Modeling and Control," Springer, London, UK, 2014.

[10] RTE, France "Voltage regulation and constructive capacities in reactive power of generation installations," Reference technical documentation, 2016. http://clients.rte-france.com/lang/fr/visiteurs/mediatheque_client/offre.jsp

[11] K.R. Padiyar "Analysis of subsynchronous resonance in power systems," Springer Science+Business Media, New York, USA, 1999.

[12] B. Wen, D. Boroyevich, P. Mattavelli, Z. Shen, and R. Burgos "Influence of Phase-Locked Loop on Input Admittance of Three-Phase Voltage-Source Converters," in the 23th Applied Power Electronics Conference and Exposition (APEC),17-21 March, Long Beach, CA, USA, pp. 897-904, 2013.